Multimillijoule, highly coherent x-ray laser at 21 nm operating in deep saturation through double-pass amplification

B. Rus,[1] T. Mocek,[1] A. R. Präg,[1] M. Kozlová,[1] G. Jamelot,[2] A. Carillon,[2] D. Ros,[2] D. Joyeux,[3] and D. Phalippou[3]
[1]*Gas Lasers Department/PALS Research Centre, Institute of Physics, Academy of Sciences of the Czech Republic, 182 21 Prague 8, Czech Republic*
[2]*Laboratoire de Spectroscopie Atomique et Ionique, Bâtiment 350, Université Paris-Sud, 91405 Orsay Cedex, France*
[3]*Institut d'Optique Théorique et Appliquée, Laboratoire Charles Fabry, Bâtiment 503, Université Paris-Sud, 91403 Orsay Cedex, France*
(Received 7 May 2002; published 12 December 2002)

The deeply saturated operation of a double-pass Ne-like zinc soft x-ray laser emitting at a wavelength of 21.2 mm is reported, along with results of a study and optimization of its beam parameters and coherence. The active medium is a 3-cm-long plasma column produced by a separately delivered prepulse and a main pulse with a duration of ~450 ps, supplied by a 1.315-μm laser. To generate plasma with reduced lateral density gradients, the ~130-μm-wide main pulse focus, producing a pump irradiance of $\sim 2.8\times 10^{13}$ W cm^{-2}, is placed on top of a much broader prepulse focus. The x-ray laser emission emerges as a narrowly collimated beam possessing high spatial quality and coherence. The dependence of the output on the prepulse conditions, the pump power, and the setup of the half-cavity mirror are investigated and discussed. The study of the beam transverse coherence demonstrates its strong dependence on pump energy. The large gain-length product attained through half-cavity operation allows for an efficient extraction of the energy stored in the active medium. With a small-signal gain of $7(\pm 0.5)$ cm^{-1}, the double-pass beam is deeply saturated and provides ~4 mJ of energy in one pulse, corresponding to peak power in excess of 40 MW, and implies that this system is the most powerful x-ray laser yet demonstrated. The inherent engineering conception of the device is compatible with a repetition rate in a hertz domain.

DOI: 10.1103/PhysRevA.66.063806 PACS number(s): 42.55.Vc, 42.60.Da, 52.50.Jm, 42.25.Kb

I. INTRODUCTION

Development of collisional x-ray lasers (XRLs) and their use for various applications is currently a diversified discipline where several approaches are being pursued in parallel [1–3]. While population inversion in all these systems is created by collisional excitation of a closed-shell or subshell ion configuration by free plasma electrons, there are significant differences in generating the plasma active medium with appropriate ionization balance, and/or its heating to the required temperature.

The first and perhaps most widespread approach, using as the active medium a plasma created and heated by transverse illumination of a solid (or gas puff) target, has been routinely implemented to produce population inversions in Ne- and Ni-like ions and intense lasing over a broad wavelength range. By using a-few-hundred-ps down to sub-100-ps pumping, saturated emission was obtained at 20.6, 23.6, 15.5, 21.2, and 25.5 nm in Se, Ge, Y, Zn, and Fe Ne-like lasers, respectively [4–8], and at 5.8, 7.3, and 13.9 nm in Dy, Sm, and Ag [9–11] Ni-like lasers. The maximum reported output from these systems—and the only one exceeding 1 mJ—was 7 mJ in Ne-like Y, using frequency-doubled multikilojoule pumping [6]. A modification of the pumping configuration, consisting in the decoupling creation of a plasma with the required ionization balance and creation of the electron temperature optimizing the excited-state kinetics, has recently made it possible to achieve saturation with pumping energy of a few joules delivered in typically picosecond pulses. Regarding the amplification lengths of about a centimeter, the experimental implementation of this transient collisional excitation (TCE) approach involves traveling-wave excitation. Using this technique, saturation has been reported at 32.6 and 19.6 nm in Ne-like Ti and Ge [12,13], and at 11.9, 13.9, 14.7, and 18.9 nm in Ni-like Sn, Ag, Pd, and Mo [14–17], the Pd laser delivering the highest output energy of ~12 μJ [16].

The second approach of generating strongly amplified soft x-ray radiation is a capillary-discharge system where the lasing medium is generated in a gas-filled capillary channel by a fast discharge current pulse. Saturated operation at 46.9 nm in Ne-like Ar has been demonstrated on this scheme [18,19], and pulses with the average energy of 0.9 mJ were generated [20]. More recently, nearly a fully coherent beam was achieved with this system using a 36-cm-long capillary [21].

The third experimentally demonstrated approach is based on optical-field ionization by ultrashort laser pulses and employs a longitudinally pumped channel in a gas cell. The plasma is generated by tunneling ionization, while the population inversion is driven by collisional excitation by the electrons passed into the continuum; the ionization and pumping are thus largely decoupled through bypassing the process of ionization cascade by free electrons. Using this scheme, lasing at 41.8 nm in Pd-like Xe [22] was reported, and saturation was achieved [23] with an estimated output energy of ~25 nJ per pulse, at a 10 Hz repetition rate.

In this work, we maintain our interest in Ne-like systems driven by multi-100-ps pulses and using solid targets. We systematically examine the optimum performance of the double-pass amplification at 21.22 mm at the transition

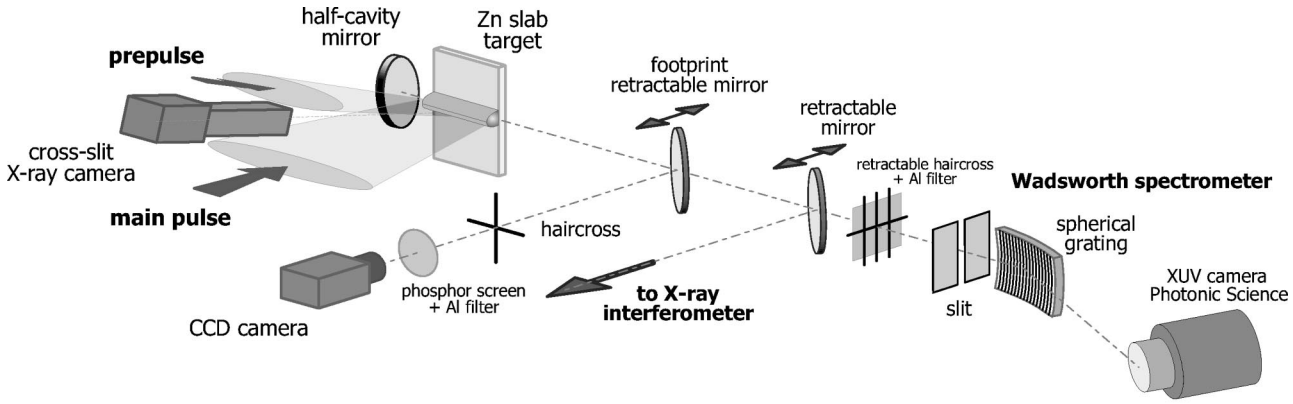

FIG. 1. Schematic experimental setup (not to scale). The cross-slit camera sits in the space between the converging laser beams and views the target under ~13° with respect to the horizontal plane. The flat half-cavity mirror is located 8.5 mm from the target edge. The spectrometer may be used both in the standard spectrally resolving mode or in a low spectral-resolution mode with the entrance slit open; in the latter case a haircross in front of the slit is employed as a spatial/dimensional fiducial.

$(2p^5_{1/2}3p_{1/2})_{J=0} \rightarrow (2p^5_{1/2}3s_{1/2})_{J=1}$ in Ne-like zinc, using a plasma column of 3 cm length. Strong lasing at this transition (henceforth labeled $J=0$-1) has been demonstrated in Ref. [24], while the fundamental role of very weak prepulses (0.01–0.1 % of the pump energy) in the functioning of this laser was identified some time later [25–27]. Saturated operation of the $J=0$-1 zinc laser using the double-pass configuration was demonstrated [7,26] and has been characterized in detail [28].

The described experiment employs a separately delivered prepulse to produce a wide preplasma column into which the main pulse, focused much more tightly, is coupled. This arrangement, thus far experimentally unexploited, allows us to produce a plasma with reduced lateral gradients and thus reduce the deleterious effects of lateral beam refraction. This adds to the known prepulse benefits consisting in an increase of the transverse size of the gain region and a reduction of the transverse density gradient, improving significantly the propagation conditions of the x-ray beam along the plasma [29]. Moreover, a prepulse may positively contribute to the beam coherence through smoothing the amplifying medium over a micrometer scale and reducing small-scale fluctuations of the local gain [30].

The investigated zinc XRL is pumped by a wavelength of 1.315 μm. This is expected to act beneficially for the performance of the system, as simulations show an enhanced efficiency of a 1.3-μm driver over the commonly used 1.06-μm pumping [31]. To achieve an efficient extraction of the population inversion, the XRL is operated in a double-pass regime.

The primary goal of this experiment was to demonstrate that a half-cavity zinc XRL pumped by multi-100-ps pulses of energy ~500 J is capable of delivering several millijoules in a narrowly peaked beam; this represents a dramatic efficiency improvement over the formerly reported multikilojoule pumping required to produce a comparable output. Another rationale was to show that the half-cavity arrangement may be implemented in a fashion compatible with a potentially high shot rate. To achieve high spatial coherence, the investigated XRL is operated in a configuration with the Fresnel number $\pi a^2/\lambda L$ close to 1 (a is the gain region size and L the optical path length in the system). We first adjust the prepulse conditions to maximize the ASE (amplified spontaneous emission) single-pass output at 21.2 nm. Subsequently, we optimize the half-cavity output with respect to both the prepulse conditions and the half-cavity geometry. The obtained results are discussed using model calculations of a saturated, bidirectional propagation ASE system.

II. EXPERIMENT

The experiment was conducted at the recently established PALS (Prague Asterix Laser System) facility [32,33]. The main experimental resource at PALS is an upgraded version of the former Asterix IV iodine laser system [34] developed at the Max-Planck-Institut für Quantenoptik (Garching). The laser provides up to 1.2 kJ at the fundamental wavelength of 1.315 μm in a typically 450-ps full width at half maximum (FWHM) pulse, in the main beam of 29 cm diameter. Additionally, up to 100 J may be delivered in the auxiliary beam of 14.8 cm diameter, having an identical temporal profile as the main beam. This beam was used here to produce a prepulse.

The experiment was deployed in the PALS tandem of vacuum target chambers of advanced conception [35]. The experimental arrangement is shown in Fig. 1. The x-ray laser amplifier is generated by irradiating a 3-cm-long target which consists of an optically polished zinc slab with a surface flatness of about 5 μm or better. One 5-cm-high target may be used about 100 times, which is achieved by its vertical translation after each shot by typically 300 μm to expose the fresh target surface to the driving beam in the subsequent shot. The target is bonded on an interchangeable lock-in support plate, and, once the target is consumed, this piece can be promptly replaced by another ''batch.''

The pump-laser sequence consists of a joule-level prepulse, followed after 10($\pm$0.5) ns by the main driving pulse delivering to the target typically 500 J (~600 J at the output of the laser) and producing a net irradiance of $\sim 2.8 \times 10^{13}$ W cm^{-2}. The prepulse beam is applied at the target at

an angle of 25° from above (see Fig. 1) and is focused down to a 40-mm-long line by a tandem of cylindrical and spherical lenses, overfilling the target in order to produce uniform prepulse conditions over the full length of 3 cm. The width of the prepulse focus was typically ~700 μm, significantly larger than the focus width of the main beam. The prepulse energy varied between 0.75 and 17 J, while its typical value was 1.6 J corresponding to a net target irradiance of $\sim 1.6 \times 10^{10}$ W cm^{-2}.

The main beam is focused by a $f/3$ composite system consisting of a matrix of ten planoconcave cylindrical lenses 150×60 mm and a single aspherical lens. It provides a highly uniform 30-mm-long line focus of ~130 μm width. The cylindrical matrix is arranged as two arrays of five lenses mounted on a support including a 10-mm-high central strut across the horizontal beam axis, protected from the laser by a stripe of absorbing glass. This arrangement is an improved version of a previous design [36], where cylindrical lenses extending over the full height of a laser beam were employed. Here, by vertically stacking two lenses, a more uniform and narrower line focus may be generated, benefiting from the possibility to cost effectively fabricate shorter cylindrical lenses with very tight specifications (parallelism of the face surfaces, parallelism of the generating axis to the side edges). The sole expense of achieving the significantly improved focus quality is almost a negligible screening effect of the central strut, amounting here to 4.5% of the total beam energy.

The lateral extent and uniformity of the plasma column, as well as the superposition and coalignment of the prepulse and the driving foci, were monitored by a cross-slit x-ray camera face viewing the target under ~13° with respect to the horizontal plane (see Fig. 1). The camera provides an astigmatic image of the plasma column in a multi-keV spectrum, with a vertical magnification of 3 and a horizontal demagnification of 4.5. An off-shelf charge-coupled device (CCD) chip stripped off the cover glass, filtered by a 3-μm Al foil, is employed as a detector.

The half-cavity is a centerpiece in achieving large amplification lengths and deeply saturated lasing. It consists of a 25-mm-diameter Mo:Si flat multilayer mirror, with a reflectivity near 21 nm of ~30% [37]. The mirror is positioned at 8.5 mm from the plasma, and is mounted on a compact five-axis support allowing to remotely control its position and orientation. The reflecting surface is protected from plasma debris by a stainless-steel shield with a 1-mm hole allowing the x-ray beam to pass, placed ~1 mm in front of the mirror. This arrangement restricts the mirror damage to an area roughly equal to the hole size, and allows one mirror to be employed for as many as 100 shots.

The emerging XRL beam was alternatively analyzed by a footprint monitor or by an x-ray spectrometer, or may be sent to an x-ray interferometer. The beam is switched between the individual diagnostics by making it reflect off the respective flat retractable multilayer mirror (Mo:Si) working at 45°.

The footprint monitor is located at a distance of 110 cm from the XRL exit plane and employs a fine-grain Tb-doped phosphor screen (Proxitronic) coated by a 40-nm Al layer to reject visible light. The signal produced on the screen is relayed by a visible imaging system to a CCD camera. A spatial fiducial consisting of a 120-μm-diameter wire haircross is positioned 22 cm in front of the phosphor.

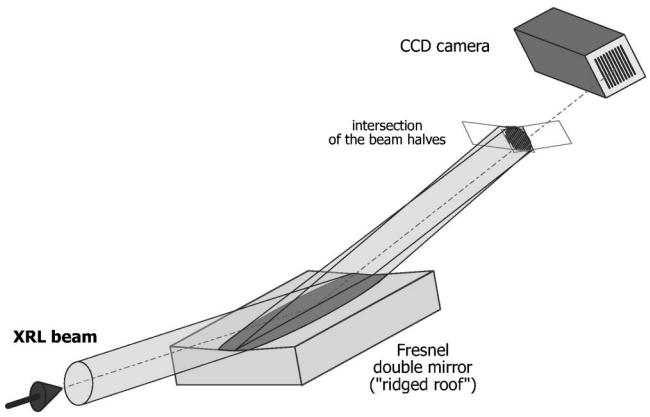

FIG. 2. Fresnel double mirror x-ray interferometer consisting of a ''ridged roof'' with the surface roughness of ~5 Å. It is positioned ~3 m downstream from the plasma exit plane via reflection on a 45° mirror. The dimension of the Fresnel double mirror is $(2 \times 15) \times 60$ mm. The camera consists of 512×512 pixels of the size 19×19 μm.

The x-ray beam is spectrally analyzed by a grazing-incidence grating spectrometer employing Wadsworth geometry [38]. A spherical blazed grating with 900 lines/mm and with a radius of curvature 4675 mm is used to focus near-parallel emission to the detector, which is an XUV imaging camera (Photonic Science) equipped with a phosphor and an optical-fiber demagnifier, butt coupled to a cooled CCD. The camera is located at 305 cm from the plasma and allows viewing a spectral window of ~40 Å. The spectrometer sits on a translation-rotation board making it possible to see the plasma under different pointing angles and thus examine the angular profile of the x-ray emission. A 1.5-μm Al filter was used to avoid saturating the detector in half-cavity shots.

The coherence analysis of the x-ray beam emitted by the half-cavity was performed using a wave-front-splitting Fresnel interferometer [39,40] (see Fig. 2), located 3 m downstream from the plasma. The interference pattern is produced by reflecting the beam at grazing incidence (here 6°) off a tandem of adjacent plane mirrors inclined to each other at a small angle (5.2 mrad). Upon crossing over, the reflected beam halves produce an interference pattern. The resulting fringes were detected by a phosphor-coated 512×512 pixel CCD camera (ARP Photonetique) located in the overlapping region of the beam halves, 70 cm downstream from the Fresnel double-mirror center. To augment the observed fringe spacing, the camera was inclined to view the fringes under a near-grazing incidence angle (6°). No filters were used in these measurements in order to maintain the wave-front quality of the emitted beam.

III. EXPERIMENTAL RESULTS

The data provided by the cross-slit x-ray camera allowed us to evaluate the size and quality of the line focus, and thereby accurately determine the plasma pump conditions

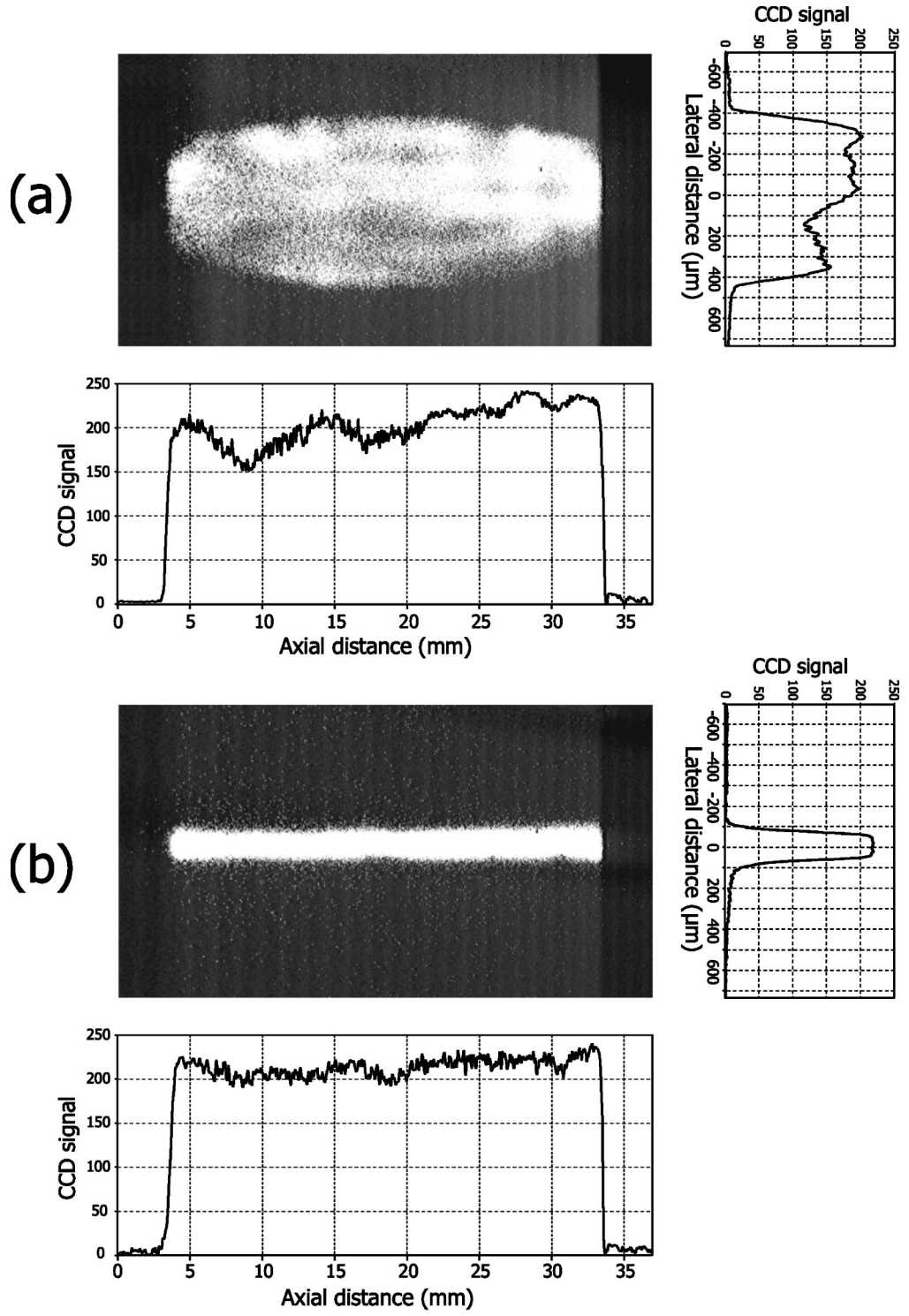

FIG. 3. Image of the plasma column in a multi-keV x-ray spectral range. (a) Preplasma emission (taken with increased energy in the prepulse beam to become visible, without firing the main pulse), (b) Image of the plasma created by the main pulse.

throughout the experiment. To discern the prepulse focus, shots with increased energy (≈60 J) in the prepulse beam were fired, in absence of the main pump beam.

A typical set of the focus x-ray images is shown in Fig. 3. The prepulse focus width is ≈ 700 μm, and in the longitudinal direction it largely overfills the target length of 3 cm. It also exhibits minor intensity fluctuations, replicating the nonuniformities of the prepulse beam. In contrast, the main pulse focus is both highly uniform and has an even, ~130 μm, width across the full length of 3 cm, illustrating the performance of the composite focusing system employed. We believe that the superior quality of the focus played a significant role in achieving the reported operation parameters of the described zinc x-ray laser.

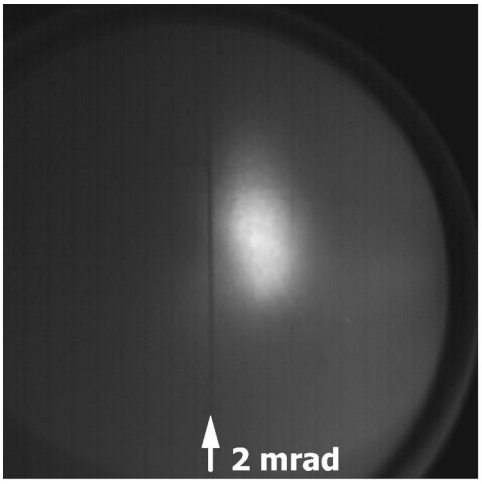

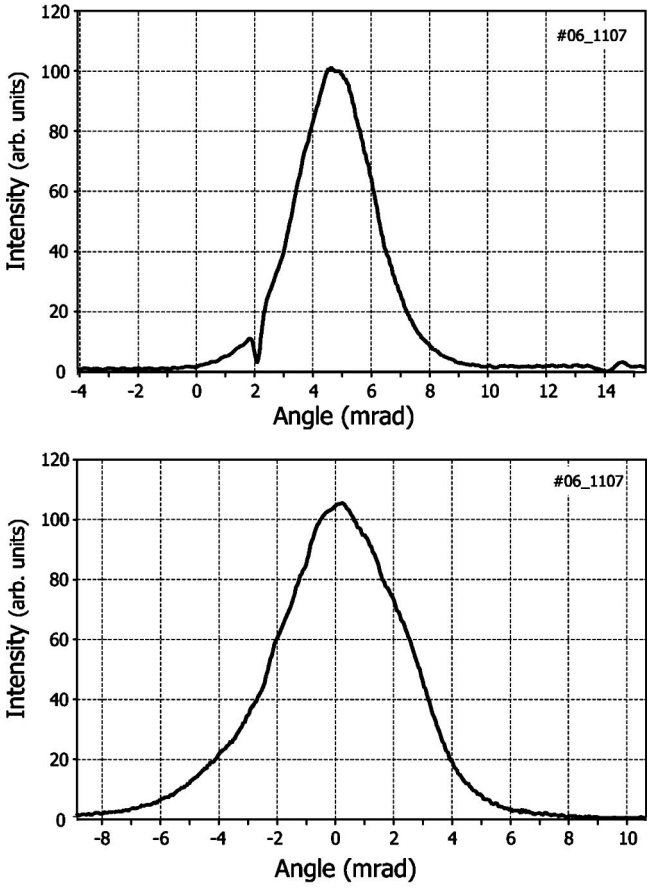

FIG. 4. Far-field pattern (footprint) of the 21.2-nm XRL beam produced in the single pass, with its horizontal and vertical densitometry profiles. The target surface is on the left side of the footprint.

A footprint of the ASE x-ray beam emergent from a 3-cm-long plasma is shown in Fig. 4, along with its intensity profiles. A smooth ellipsoidal beam possessing a high degree of both horizontal and vertical symmetry is produced, with respective divergences of $3(\pm 0.5)$ and $5(\pm 0.5)$ mrad. The beam is emitted from the plasma at an angle of $5(\pm 0.5)$ mrad with respect to the target surface. This pointing angle was observed to be only weakly dependent on the driving laser energy.

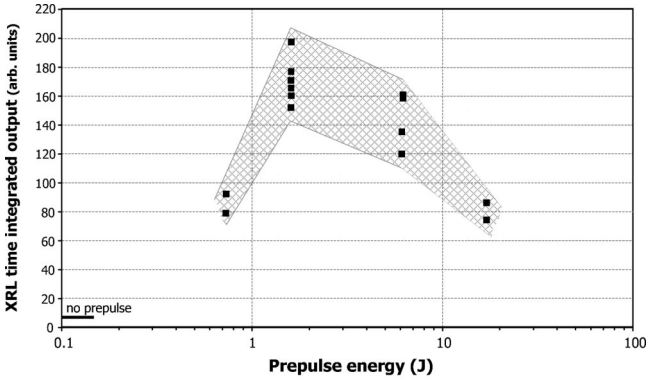

FIG. 5. The 21.2-nm XRL single-pass output as a function of the prepulse energy; the error bar space is represented by a shaded region for clarity. The optimum prepulse energy 1.6 J corresponds to a net target irradiance of $\approx 2\times 10^{10}$ W cm^{-2}.

The laser signal at 21.2 nm was completely dominating the emitted spectrum, which allowed us to use the camera coupled to the spectrometer to assess the number of photons contained in the x-ray beam. To this goal, the spectrometer entrance slit was opened to $\sim$10 mm to collect the whole beam, and the detector was slightly moved away from the focusing circle to receive nonfocused emission over a large area. Upon converting the signal thus received via the quantum efficiency of the phosphor and other characteristics of the Photonic Science camera, the number of soft x-ray photons generated in the single-pass ASE regime is estimated to be in excess of 10^{13}, indicating saturated operation.

The dependence of the x-ray laser output on the prepulse was examined for prepulse energies ranging from 0.75 to 17 J, while the prepulse focus conditions, as well as all characteristics of the main beam, were kept unchanged. The obtained dependence of the emerging x-ray signal is displayed in Fig. 5, containing both single-pass ASE and double-pass data. These show that the performance of the studied x-ray laser is optimized, under the given experimental conditions, for a prepulse energy of 1.6 J, which corresponds to a net irradiance of $\sim 1.6\times 10^{10}$ W cm^{-2} or to the prepulse-to-main-pulse irradiance ratio of $\sim 6\times 10^{-4}$. We note that this observation of a specific weak prepulse optimizing a zinc laser corroborates the former results obtained using a different experimental setup [41]. A similar prepulse dependence was also observed in the Ni-like Ag laser [11], in contrast with some other x-ray lasers apparently exhibiting a monotonic dependence of the output on the prepulse.

Upon activating the half-cavity mirror, the x-ray laser output from a 3-cm plasma is boosted typically 11 times, although it moderately depends on the angle under which the beam reflected from the mirror is reinjected back into the plasma for return amplification.

Figure 6 displays a footprint record of the double-pass beam emitted in the optimum half-cavity configuration, at the reinjection angle of 1 mrad (see below). The beam emerges from the plasma under an angle of $\sim$5 mrad and its

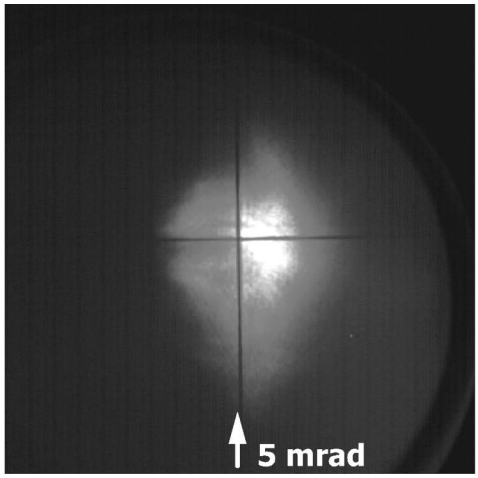

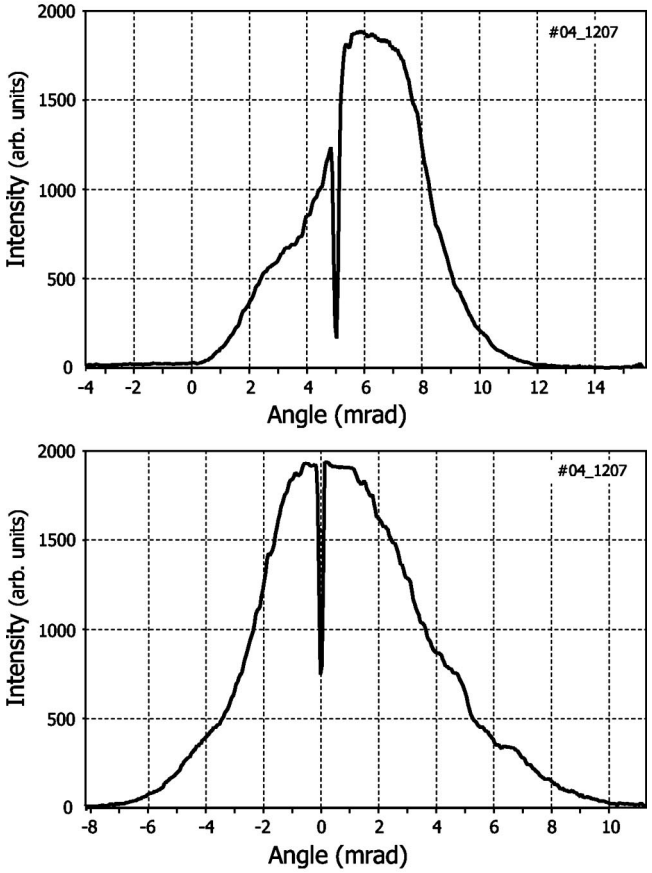

FIG. 6. Far-field pattern (footprint) of the double-pass XRL beam, with its horizontal and vertical densitometry profiles. The target surface is on the left side of the footprint.

horizontal and vertical divergences of $3.8(\pm 0.5)$ and $5.8(\pm 0.5)$ mrad, respectively, are close to those of the single-pass ASE.

Regarding the radiation transit time of 256 ps in the half-cavity, non-negligible with respect to the 450-ps pump pulse duration, it was essential to establish whether the gain lifetime allows the backward-propagating radiation to be amplified over its whole path in the plasma. To check whether the gain fades out or not during the return pass in the half-cavity, several shots with different lengths of the pump pulse were fired. The results are shown in Fig. 7.

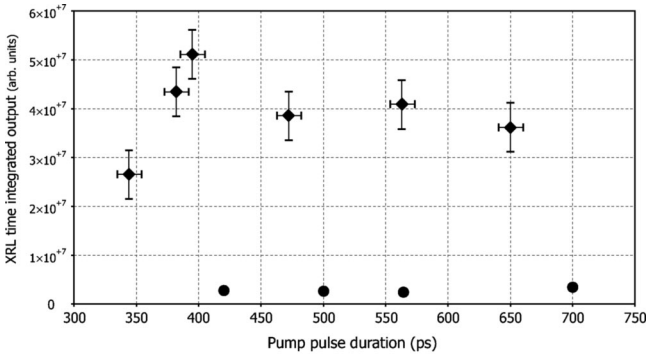

FIG. 7. The single- (●) and double-pass (♦) 21.2-nm output as a function of the duration (power) of the pump pulse. The significantly plummeted double-pass signal for a 344-ps pulse indicates gain duration being shorter than the radiation transit time in the half-cavity.

The XRL output corresponding to single-pass ASE exhibits a moderate dependence on the pump pulse, decreasing slightly with its duration as a result of decreasing pump power. This relatively weak dependence on the pump power suggests again that the x-ray laser emission produced by a single pass is saturated. A similar behavior is observed for the double-pass output, except for the pump pulse of 344 ps (the shortest that can be presently generated at PALS) resulting in an abruptly lowered XRL output, which was also the lowest half-cavity XRL signal obtained in the whole experiment. This drop-off behavior is a clear-cut indication that the gain duration for 344-ps pumping is shorter than the x-ray radiation transit time in the half-cavity, while the gain driven by a 450-ps pump lasts sufficiently enough to fully sustain the return amplification. The character of the double-pass data also shows that the mirror maintains its reflectivity over the duration of the x-ray pulse.

The half-cavity configuration was optimized with respect to the reinjection angle under which the ASE emission was reflected back to the plasma for return amplification. The obtained footprints corresponding to reinjection angles α_r of -3, 1, 5, and 9 mrad (the mirror tilt Φ being 1, 3, 5, and 7 mrad, respectively) are displayed in Fig. 8(a). From Figs. 8(b) and 8(c), showing the XRL beam divergence and its intensity as a function of the reinjection angle, it is apparent that both the intensity and the beam spatial quality are simultaneously optimized for the reinjection angle $\alpha_r = 1$ mrad (although a comparable intensity is produced for $\alpha_z = 5$ mrad). Also, from Fig. 8(a) it is seen that the refraction angle is nearly independent of the reinjection angle, retaining a value of $5(\pm 0.5)$ mrad, which is identical, within the experimental precision, to the pointing angle of the single-pass ASE beam. These observations, providing important insights into the morphology of the gain region, are further discussed in Sec. IV.

A typical interferogram produced by the half-cavity beam, using the Fresnel wave-front-splitting interferometer, is shown in Fig. 9. The fringe straightness and contrast, appar-

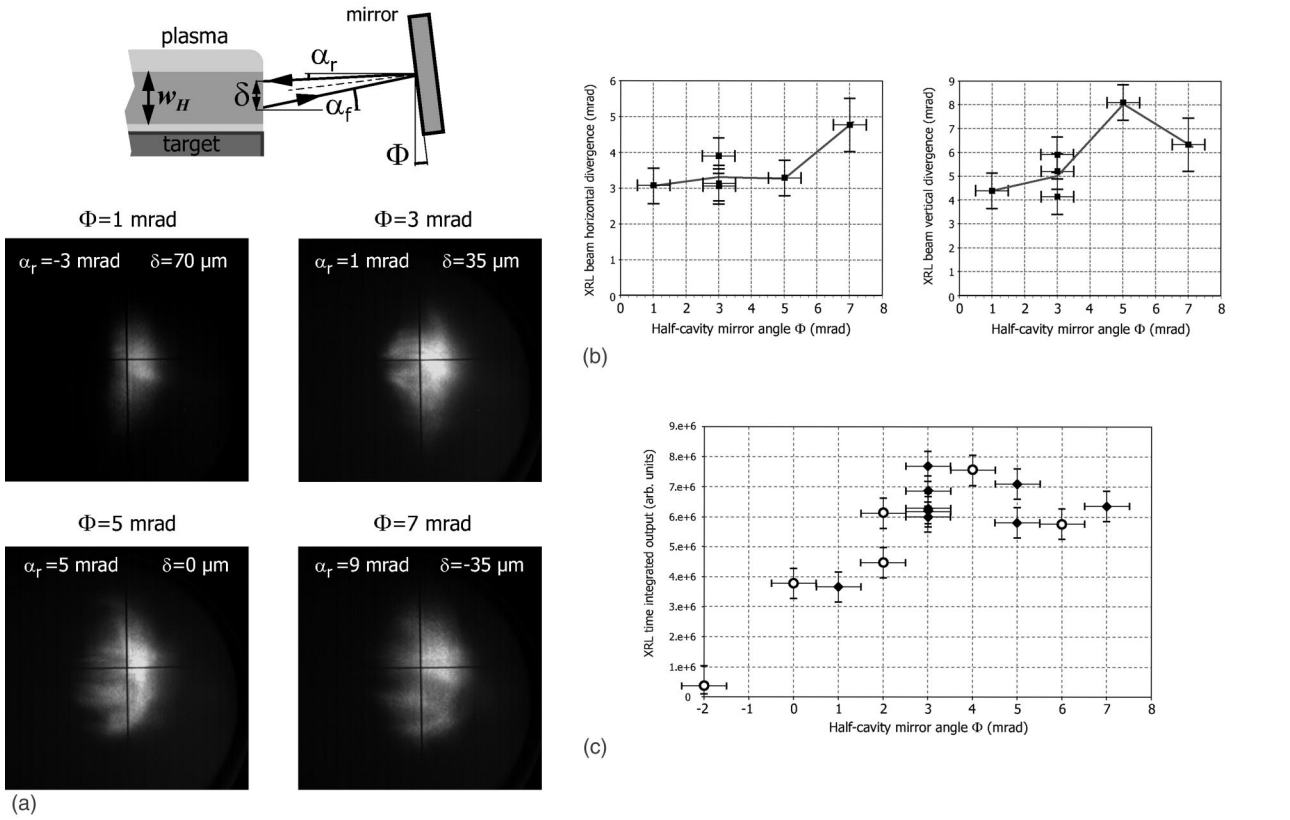

FIG. 8. The half-cavity output as a function of the mirror azimuth angle Φ: a ray emerging from the plasma under a forward angle α_f is reflected back under an angle $\alpha_r = 2\Phi - \alpha_f$, and reenters the plasma at a distance $\delta \sim 2D(\alpha_f - \Phi)$ with respect to the emerging point; w_H is the horizontal size of the gain region. (a) The x-ray beam footprints for $\Phi = 1$, 3, 5, and 7 mrad (the haircross vertical wire is positioned at 5 mrad), (b) the horizontal and vertical divergence as a function of the reinjection angle, (c) the output intensity as a function of the reinjection angle (♦ and ○ are the data from the footprint monitor and from the XUV spectrometer, respectively).

ent from the interferogram lineout, demonstrate both a good beam wave-front quality and high spatial coherence of this x-ray laser.

The visibility of the fringes, $(S_{\max} - S_{\min})/(S_{\max} + S_{\min})$, where the signals $S_{\max}$ and $S_{\min}$ correspond to the maximum and adjacent minimum in the fringe system, was inferred after subtracting from the raw interferograms a background signal of a value carefully determined for each shot. The analysis included no further processing tending to artificially enhance the interferogram quality. The error bars, estimated conservatively at ± 0.05, correspond to the uncertainty in the determination of the background signal (mostly due to visible light penetrating the CCD) and to the variation of the visibility across the interferogram.

The dependence of the fringe visibility on the net pumping energy is shown in Fig. 10. The data clearly show that the coherence of the x-ray beam increases with the pump energy (and thereby pump power). The highest fringe visibility achieved under the given experimental configuration amounts to 0.51. On the other hand, the data, collected for several days, exhibit a notable scatter, which was observed to occur especially on a day-to-day basis. The origin of this scatter, which is in stark contrast to the reproducibility of the x-ray laser output intensity, is not clear; it may however be at least partially attributed to the rising edge shape of the pump laser, which was observed to vary during this particular series of shots.

IV. DISCUSSION

The x-ray laser output generated both by the single and the double pass was observed to be largely robust with respect to different pumping conditions. It equally exhibited an excellent reproducibility after an exchange of the target and/or of the half-cavity mirror.

One of the parameters determining the output beam is the trajectory along which the emission reflected from the half-cavity mirror is fed back into the plasma for return amplification, as seen from Fig. 8. When the ASE beam is reflected into a low-density plasma further away from the target, the emerging output beam is a moderately amplified, refraction-unaffected duplicate profile of the ASE seed. As the reflected ASE emission is injected closer to the target, it samples a higher gain but suffers from refraction and the output beam profile is unlike the ASE beam shape. The pointing angle of the output beam is however essentially independent of the reinjection conditions, implying that its intensity reflects the gain magnitude at the sampled distance from the target. This makes it possible to assess the transverse size of the gain region, using the data from Fig. 8.

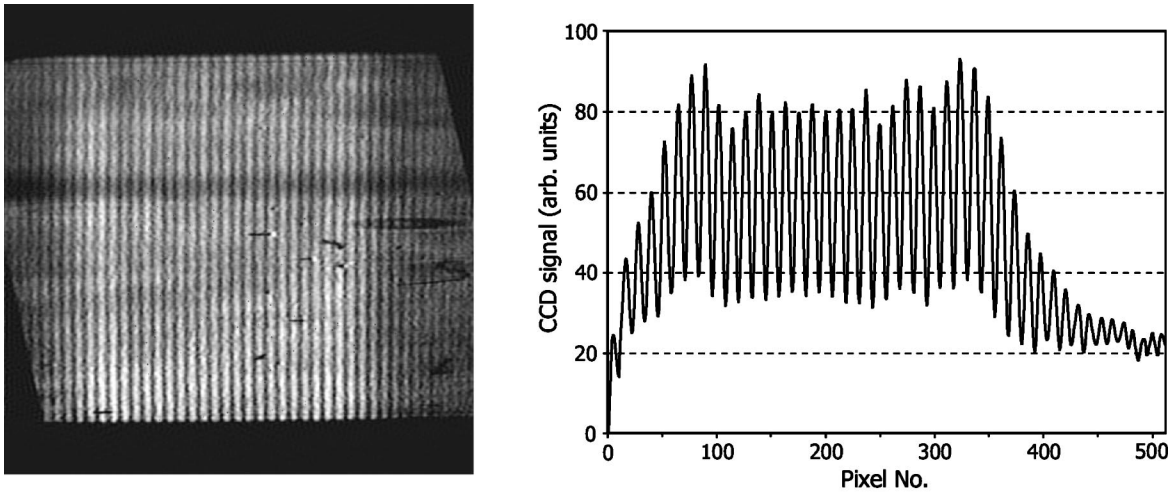

FIG. 9. Interference fringe pattern produced by the half-cavity beam and the Fresnel double-mirror interferometer, and an averaged lineout taken across the fringes. The XRL beam vertically overfills the mirror (cf. Fig. 2), and its horizontal dimension is ~11.5 mm. The defects in the raw CCD record are due to microscratches on the conversion phosphor. The visibility of the fringes in the central part of the beam amounts here to 0.43(±0.05).

Assuming that the ASE beam with a horizontal divergence ϕ_H emerges from an active region of size ω_H, upon reflection at the half-cavity mirror this beam will reenter the plasma expanded in size to $w_H+2D\phi_H$, where D is the distance plasma mirror. To produce an intense double-pass output, the seeded beam must non-negligibly overlap with the gain region, which will typically occur for reinjection positions extending over a distance equal to the seed beam size, i.e., $w_H+2D\phi_H$ (assuming a static gain region overlapped at least by 50% by the seed beam). Using $\phi_H = 3$ mrad, $D=8.5$ mm, and the data from Fig. 8, which show that comparable x-ray outputs are produced for reinjection distances δ scanned over ≈ 100 μm, we obtain $w_H \approx 50$ μm.

The feedback provided by the half-cavity mirror, which we define here as the fraction of the ASE output returned back to the plasma for further amplification, can be evaluated as the reflected fraction of the x-ray beam overlapping the gain region of the plasma. Due to refraction, not all rays arriving at the gain region at the plasma entrance plane will propagate and receive amplification over the full return length, and the actual value of feedback for the surviving ray bundles will be given by considering the overlap plane someplace inside the plasma. By labeling the mirror reflectivity R (the ''raw'' spectral reflectivity at the given wavelength) and the geometric coupling efficiency, C_g, the feedback F in the case of a plane mirror can be expressed as

$$F = RC_g = R\frac{w_H w_V}{[w_H(2D+d)\phi_H][w_V+(2D+d)\phi_V]}, \quad (1)$$

where w and ϕ denote gain region size and beam divergence in the horizontal and vertical directions according to the subscripts, and d is the distance of the overlap plane from the plasma end. Taking $w_H \approx 50$ μm, $w_V \approx 130$ μm, $\phi_H \approx 3$ mrad, $\phi_V = 5$ mrad, $R=0.3$, $D=8.5$ mm, the feedback amounts to $F=0.087$ when $d=0$ mm, and $F=0.027$ for $d=30$ mm. The actual feedback lies between these extreme values, and we may take as its best estimate the average of these two values, i.e., $F=5.8\times10^{-2}$.

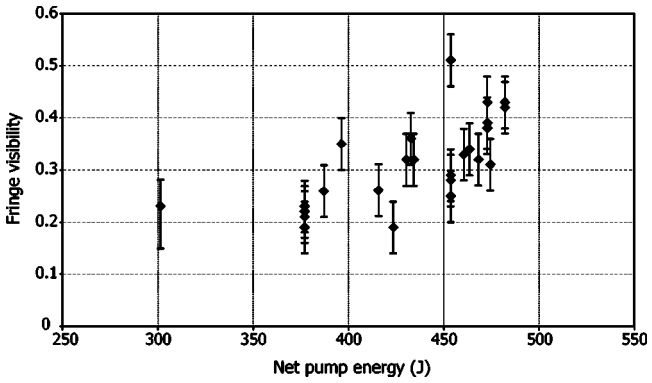

FIG. 10. Visibility of the interferometric fringes generated by the half-cavity, as a function of the net pump energy. The vertical error bars reflect visibility variation across the central part of the interferograms.

The observed 11× enhancement of the x-ray output in the half-cavity configuration with respect to the single pass provides additional evidence that the laser is strongly saturated. Given that the x-ray beam receives amplification over the full return path, the output I_{dp} in the small-signal gain regime would approximately (neglecting the effects of spectral narrowing by gain) amount to

$$I_{dp} \approx I_{sp}[F\exp(g_0 L)+1], \quad (2)$$

where I_{sp} denotes the single-pass output, F is the feedback defined above, L is the plasma length, and where it is assumed that the small-signal gain g_0 has an identical value for the forward and return pass. Assuming the feedback $F=5.7$

$\times 10^{-2}$, for $L=3$ cm we obtain $g_0=1.87\ \mathrm{cm}^{-1}$. This value is clearly inconsistent both with the number of photons (larger than 10^{13} emitted in the single pass) estimated from the spectrometer detector, and also with the high coherence of the emitted beam, indicating that the system operates in a deep saturation.

To quantitatively determine the performance of the studied x-ray laser with respect to the saturation intensity of the amplifying plasma, we carried out simplified modeling of radiation transfer in an active medium that is representative of the experimental situation encountered. The model, described in detail elsewhere [42], treats time-dependent bidirectional amplification of axial emission in a refraction-free active medium, and accounts in full for the transfer of the spectral line profile. It is assumed that both the small-signal emissivity and the small-signal gain (given by the atomic kinetics rates in absence of the amplified radiation) are constant along the amplifier axis z; let j_0 and g_0 denote their peak spectral values. By labeling with I^+ and I^- the emission propagating in the positive and negative z direction, respectively, the basic equation of the model can be expressed as

$$\frac{\partial I^{\pm}(z,t,\nu)}{c\,\partial t} \pm \frac{\partial I^{\pm}(z,t,\nu)}{\partial z} = \frac{j_0(t,\nu)}{1+\dfrac{I_{\mathrm{tot}}(z,t)}{I_{\mathrm{sat}}(t)}} + \frac{g_0(t,\nu)I^{\pm}(z,t,\nu)}{1+\dfrac{I_{\mathrm{tot}}(z,t)}{I_{\mathrm{sat}}(t)}}, \qquad (3)$$

where

$$I_{\mathrm{tot}}(z,t)=\int_{-\infty}^{+\infty}[I^+(z,t,\nu')+I^-(z,t,\nu')]\,d\nu' \qquad (4)$$

is the spectrally integrated sum intensity of the right- and left-going emission, and $I=h\nu_0/\sigma\tau_R$ is the saturation intensity involving the spectral peak frequency ν_0, the cross section of the stimulated emission σ, and the gain recovery time τ_R. The saturation intensity depends on the plasma conditions solely–and weakly–through τ_R.

The feedback provided by the half-cavity mirror, sitting at a distance D left from the plasma (see Fig. 1), enters into Eq. (3) as a boundary condition. Specifically,

$$I^+(z=0,t,\nu)=FI^-(z=0,t-2D/c,\nu), \qquad (5)$$

The validity of the model was examined using a previously reported half-cavity Zn laser [28] as a testbed, employing therein experimentally determined time profiles of the emissivity and gain. Despite the relative simplicity of the model, a remarkably good agreement between the calculated and measured time evolution of the x-ray laser output signal for different half-cavity configurations was found [42].

The Zn laser reported in this work was modeled using time evolution of the small-signal emissivity and gain according to those established experimentally for Ne-like Zn in a previous measurement of the time characteristics of nonsaturated output produced by plasmas of different lengths [24] (for details and discussion see Ref. [42]). Specifically, the emissivity was assumed here as 50-ps flat top, linearly rising over 50 ps and decreasing exponentially to $\frac{1}{10}$ of the peak value over 200 ps, while the gain profile included a rising edge of 50 ps to a constant peak value lasting 200 ps and followed by a linear decrease down to zero over 150 ps (the influence of different time profiles on the output of the x-ray laser is discussed in Ref. [42]). The peak values of the small-signal emissivity and gain were taken as parameters to adjust the calculated ratios of the outputs from different amplification lengths to those found experimentally. The saturation intensity was $I_{\mathrm{sat}}=1.5\times 10^{10}\ \mathrm{W\,cm^{-2}}$, which is a value resulting from atomic constants and rates pertinent to Zn^{20+} under appropriate plasma parameters.

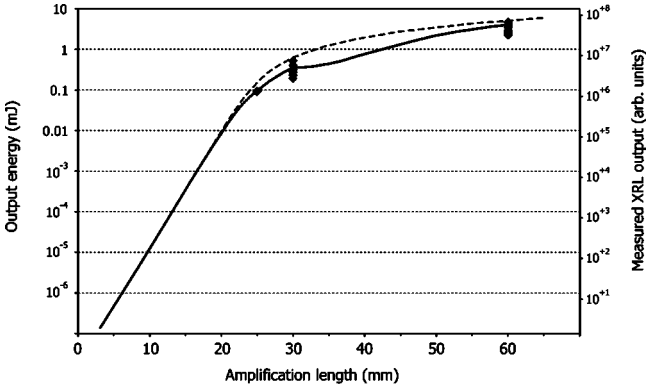

FIG. 11. The XRL output versus amplification length. For clarity only a few experimental points of those collected are represented, but include the extreme values obtained for each amplification length. The solid line represents a full bidirectional simulation of a half-cavity system and corresponds to a small signal gain of $7.0(\pm 0.5)\ \mathrm{cm}^{-1}$ (see text). For comparison, the dashed line shows the intensity-length dependence of a simple, continuous ASE amplifier with unidirectional radiation propagation.

The small-signal emissivity and gain best fitting the measured ratios of the x-ray signal between different amplification lengths (25, 30, and 60 mm) is $1.5(\pm 1.0)\times 10^4\ \mathrm{W\,cm^{-2}}$ and $7.0(\pm 0.5)\ \mathrm{cm}^{-1}$, respectively. It is worth noting that, because of the strong saturation, both the calculated magnitudes of the output intensities and their ratios are only weakly sensitive to the emissivity value. The calculated curve of the x-ray output as a function of the amplification length, corresponding to these emissivity and gain values, is shown in Fig. 11, along with the experimental data from the x-ray spectrometer. The results confirm that the laser is deeply saturated, with the equivalent small-signal gain-length product $2g_0L+\ln(F)$ amounting to ≈ 39. By integrating the real (i.e., progressively reduced by saturation) gain over the amplification length $2L$, we obtain the full-signal gain-length product of ~ 21. The simulations equally confirm that the half-cavity output is, under the given experimental conditions, nearly independent of the exact value of the feedback introduced by the mirror.

The calculated duration of the x-ray output pulse is $90(\pm 10)$ ps FWHM. Taking into account the exit aperture of $50\times 130\ \mu$m pertaining to single-pass output, the energy contained in one pulse is ~ 4 mJ corresponding to ~ 3

TABLE I. Parameters of the 21.2-nm beam emitted by the half-cavity.

Wavelength	21.22 nm
Output pulse energy	4 mJ
Number of photons per pulse	4×10^{14}
Output pulse duration	$90(\pm10)$ ps
Peak power	40 MW
Beam divergence ($h\times v$)	3.5×5.5 mrad
Peak spectral brightness ($\Delta\lambda/\lambda=10^{-3}$)	10^{27} photons s^{-1} mm^{-2} $mrad^2$
No. of shots with one target/mirror	~100

$\times10^{14}$ x-ray laser photons. This value corroborates the number of photons estimated from the data of the spectrometer Photonic Science CCD camera, and regarding the accuracy of the assessed size of the gain region, it presents a rather conservative estimate of the actual output.

V. SUMMARY

The presented half-cavity based x-ray laser at 21.2 nm delivers stable output parameters over a broad range of pumping conditions. The 450-ps duration of the pump pulse has been found adequate to maintain the population inversion over the radiation round trip in the laser consisting of a 3-cm plasma and a mirror distance of 8.5 mm. This made it possible to achieve an amplification length of 6 cm (with a minor effective reduction due to the loss on the mirror), and resulted in a deeply saturated XRL operation supplying 4 mJ of energy in pulses shorter than $\sim$100 ps, equivalent to the peak power in excess of 40 MW. To our knowledge, this is the highest peak power achieved by an x-ray laser to date.

The main parameters of the half-cavity XRL output are summarized in Table I. The pulse duration was not measured and is estimated from the double-pass saturated amplification modeling, the validity of which was checked using, as a tested, a double-pass Zn laser with an experimentally known time-resolved output [28].

The achieved results illustrate that multi-100-ps pumped soft-x-ray lasers currently offer by far the highest output energy in the given spectral domain, delivered in a high-quality beam. Accordingly, these ''quasisteady state'' lasing systems constitute a specific laser class having different assets than the TCE x-ray lasers. While their pumping needs are currently incompatible with the available tabletop drivers and their scaling down to significantly shorter wavelengths appears unrealistic, they offer multimillijoule, controllable output possessing characteristics of a true laser beam in the conventional sense.

The half-cavity using a flat multilayer mirror has become a routine component of the experiment. We were able to stack up the individual impact areas of 1 mm diameter (facing the plasma during the shot and damaged by plasma debris afterwards) in a way that allows us to perform about 100 shots using one single mirror. By benefiting from a compact, appropriately engineered automated mirror stage, the alignment of the flat mirror was extremely simple and its repositioning between subsequent shots could be performed in effectively less than 1 s. Accordingly, the described x-ray laser is, in principle, capable of operation at 1 Hz or at an even higher frequency, and its present repetition rate is determined solely by the driving IR laser.

We suppose that the performance of the XRL reported in this paper may be further improved by the optimizing parameters of the prepulse. This would be possibly accomplished by using a longer separation between the prepulse and the main pulse than 10 ns, and/or by using an appropriately timed sequence of prepulses [8,28]. A possible improvement should also be made through shaping the distribution of the intensity of the prepulse focus, especially in the lateral direction. Our future experiment will address these issues.

A topic remaining to be fully understood is the observed behavior of the transverse coherence of the XRL beam. Whilst the obtained data clearly show a strong overall increase of the beam coherence with the pump energy (and thereby with the small-signal gain), they also exhibit a significant shot-to-shot scatter which does not correlate with (minor) fluctuations of any other measured XRL parameter. No correlation with small shot-to-shot variations of the pump pulse FWHM duration was found either. Whereas an increase of the coherence with an increasing gain coefficient, generated due to stronger pumping, is expected and was predicted theoretically [43], the reasons for the shot-to-shot fluctuations remain unidentified. We suspect that a possible explanation may involve fluctuations of an early rising edge of the pump pulse and/or microscopic variations of the target surface. We however note that significant shot-to-shot fluctuations of the beam coherence were also observed in the discharge-pumped Ne-like Ar laser [44], possibly implying that this phenomenon may reflect rather fundamental aspects of the coherence build-up in ASE systems.

The characteristic applications of the described 21.2-nm laser will be able to benefit from the combination of the high pulse energy and the beam quality including coherence. As a precursor application, we have successfully exploited this laser at PALS for interferometric probing of solid-state surfaces subjected to strong electrical fields [45]. Other prepared interferometric applications include probing of laser-produced plasmas and of solid surfaces subjected to strong radiation fields [35]. The large energy and peak power available will make it possible to perform experiments devoted, for instance, to soft x-ray ablation of solids, volumetric plasma heating by soft x-ray radiation, or probing large-size plasmas and surfaces.

ACKNOWLEDGMENTS

The authors acknowledge the PALS laser facility staff, especially B. Králiková, P. Maroušek, J. Skála, and J. Ullschmied, for providing support for this experiment. We thank M. Hudeček, J. C. Lagron, and L. Cibulka for excellent design engineering, M. Soukup, V. Vomlel, J. Stránský, and J. Zeman for manufacturing the key mechanical parts of the experimental hardware, and J. Moravec from Foton s.r.o. for expertise in the implementation of the x-ray CCD camera. The multilayer mirrors used in this work were fabricated by J. Sobota of the Institute of Scientific Instruments (Brno, Czech Republic). Finally, support from K. Rohlena, K. Jungwirth, and P. Jaeglé is greatly appreciated. This work partially benefited from the EU Transnational Access to Research Infrastructures, Grant No. HPRI-00108, the National Research Center, Project No. LN00A100, and the Czech Academy of Sciences, Grant No. A1010014.

[1] *X-Ray Lasers 1998, Proceedings of the 6th International Conference on X-ray Lasers*, edited by Y. Kato, H. Takuma, and H. Daido, IOP Conf. Proc., No. 159 (IOP, Bristol, 1999).

[2] *X-Ray Lasers 2000, Proceedings of the 7th International Conference on X-ray Lasers*, edited by G. Jamelot, C. Möller, and A. Klisnick, J. Phys. IV **11**, 2 (2001).

[3] J. J. Rocca, Rev. Sci. Instrum. **70**, 3799 (1999).

[4] B. MacGowan, L. B. DaSilva, D. J. Fields, C. J. Keane, J. A. Koch, R. A. London, D. L. Matthews, S. Maxon, S. Mrowka, A. L. Osterheld, J. H. Scofield, G. Shimkaveg, J. E. Trebes, and R. S. Walling, Phys. Fluids B **4**, 2326 (1992).

[5] A. Carillon, H. Z. Chen, P. Dhez, L. Dwivedi, J. Jacoby, P. Jaeglé, G. Jamelot, J. Zhang, M. H. Key, A. Kidd, A. Klisnick, R. Kodama, J. Krishnan, C. L. S. Lewis, D. Neely, P. Norreys, D. O'Neill, G. J. Pert, S. Ramsden, J. P. Raucourt, G. J. Tallents, and J. Uhomoibhi, Phys. Rev. Lett. **68**, 2917 (1992).

[6] L. B. DaSilva, B. J. MacGowan, S. Mrowka, J. A. Koch, R. A. London, D. L. Matthews, and J. H. Underwood, Opt. Lett. **18**, 1174 (1993).

[7] P. Jaeglé, A. Carillon, P. Dhez, P. Goedtkindt, G. Jamelot, A. Klisnick, B. Rus, P. Zeitoun, S. Jacquernot, D. Mazataud, and A. Mens, in *X-Ray Lasers 1994*, edited by D. C. Eder, and D. L. Matthews, AIP Conf. Proc. No. 332 (AIP, New York, 1994), p. 25.

[8] F. Loewenthal, R. Tommasini, and J. E. Balmer, Opt. Commun. **154**, 325 (1998).

[9] G. J. Tallents, J. Y. Lin, R. Smith, A. G. MacPhee, E. Wolfrum, J. Zhang, G. Eker, R. Keenan, C. L. S. Lewis, D. Neely, R. M. N. O'Rourke, G. J. Pert, S. J. Pestehe, and J. S. Wark, in *The 6th International Conference on X-Ray Lasers, 1998*, edited by Y. Kato, H. Takuma, and H. Daido, IOP Conf. Proc. No. 159 (IOP, Bristol, 1999), p. 59.

[10] J. Zhang, A. G. MacPhee, J. Lin, E. Wolfrum, R. Smith, C. Danson, M. H. Key, C. L. S. Lewis, D. Neely, J. Nilsen, G. J. Pert, G. J. Tallents, and J. S. Wark, Nature (London) **276**, 1097 (1997).

[11] S. Sebban, H. Daido, N. Sakaya, Y. Kato, K. Murai, H. Tang, Y. Gu, G. Huang, S. Wang, A. Klisnick, P. Zeitoun, F. Koike, and H. Takenaka, Phys. Rev. A **61**, 043810 (2000).

[12] P. V. Nickles, V. N. Shlyaptsev, M. Kalashnikov, M. Schnürer, I. Will, and W. Sandner, Phys. Rev. Lett. **78**, 2748 (1997).

[13] P. J. Warwick, C. L. S. Lewis, M. P. Kalashnikov, P. V. Nickles, M. Schnürer, A. Behjat, A. Demir, G. J. Tallents, D. Neely, E. Wolfrum, J. Zhang, and G. J. Pert, J. Opt. Soc. Am. B **15**, 1808 (1998).

[14] A. G. MacPhee, R. M. N. O'Rourke, C. L. S. Lewis, J. Y. Lin, A. Demir, G. J. Tallents, J. Collier, D. Neely, D. Ros, P. Zeitoun, S. P. McCabe, P. Simms, and G. J. Pert, in *Proceedings of the 6th International Conference on X-Ray Lasers, 1998* (Ref. [9]), p. 75.

[15] A. Klisnick, P. Zeitoun, D. Ros, A. Carillon, P. Fourcade, S. Hubert, G. Jamelot, C. L. S. Lewis, A. G. MacPhee, R. M. N. O'Rourke, R. Keenan, P. V. Nickles, K. Janulewicz, M. Kalashnikov, J. Warwick, J. C. Chanteloup, A. Migus, E. Salmon, C. Sauteret, and J. P. Zou, J. Opt. Soc. Am. B **17**, 1093 (2000).

[16] J. Dunn, Y. Li, A. L. Osterheld, J. Nilsen, J. R. Hunter, and V. N. Shlyaptsev, Phys. Rev. Lett. **84**, 4834 (2000).

[17] Y. Li, J. Dunn, J. Nilsen, T. W. Barbee, A. Osterheld, and V. N. Shlyaptsev, J. Opt. Soc. Am. B **17**, 1098 (2000).

[18] J. J. Rocca, D. P. Clark, J. L. A. Chilla, and V. N. Shlyaptsev, Phys. Rev. Lett. **77**, 1476 (1996).

[19] A. Ben-Kish, M. Shuker, R. A. Nemirovsky, A. Fisher, A. Ron, and J. L. Schwob, Phys. Rev. Lett. **87**, 015002 (2001).

[20] C. D. Macchietto, B. R. Benware, and J. J. Rocca, Opt. Lett. **24**, 1115 (1999).

[21] Y. Liu, M. Seminario, F. G. Tomasel, C. Chang, J. J. Rocca, and D. T. Atwood, Phys. Rev. A **63**, 033802 (2001).

[22] B. E. Lemoff, G. Y. Yin, C. L. Gordon III, C. P. J. Barty, and S. E. Harris, Phys. Rev. Lett. **74**, 1574 (1995).

[23] S. Sebban, R. Haroutunian, P. Balcou, G. Grillon, A. Rousse, S. Kazamias, T. Marin, J. P. Rousseau, L. Notebaert, M. Pittman, J. P. Chambaret, A. Antonetti, D. Hulin, D. Ros, A. Klisnick, A. Carillon, P. Jaeglé, G. Jamelot, and J. F. Wyart, Phys. Rev. Lett. **86**, 3004 (2001).

[24] B. Rus, A. Carillon, B. Gauthé, P. Goedtkindt, P. Jaeglé, G. Jamelot, A. Klisnick, A. Sureau, and P. Zeitoun, J. Opt. Soc. Am. B **11**, 564 (1994).

[25] G. F. Cairns, M. J. Lamb, C. L. S. Lewis, A. G. MacPhee, D. Neely, P. Norreys, M. H. Key, C. Smith, S. B. Healy, P. B. Holden, G. Pert, and J. A. Plowes, in *X-Ray Lasers, 1994* (Ref. [7]), Proc. No 332, p. 289.

[26] B. Rus, A. Carillon, P. Dhez, B. Gauthé, P. Goedtkindt, P. Jaeglé, G. Jamelot, A. Klisnick, M. Nantel, and A. Sureau, in *X-Ray Lasers, 1994* (Ref. [7]), p. 152.

[27] E. E. Fill, Y. Li, D. Schlögl, J. Steingruber, and J. Nilsen, Opt. Lett. **20**, 374 (1995).

[28] B. Rus, A. Carillon, P. Dhez, P. Jaeglé, G. Jamelot, A. Klisnick, M. Nantel, and P. Zeitoun, Phys. Rev. A **55**, 3858 (1997).

[29] J. Nilsen, B. J. MacGowan, L. B. DaSilva, and J. C. Moreno, Phys. Rev. A **48**, 4682 (1993).

[30] R. Cauble, L. B. DaSilva, T. W. Barbee, Jr., P. Celliers, C. Decker, R. A. London, J. C. Moreno, J. E. Trebes, A. S. Wan, and F. Weber, Science **273**, 1093 (1996).

[31] P. B. Holden and G. J. Pert, J. Phys. B: At. Mol. Opt. Phys. **29**, 2151 (1996).
[32] B. Rus, K. Rohlena, J. Skála, B. Králiková, K. Jungwirth, J. Ullschmied, K. J. Witte, and H. Baumhacker, Laser Part. Beams **17**, 179 (1999).
[33] K. Jungwirth, A. Cejnarová, L. Juha, B. Králiková, J. Krása, E. Krouský, P. Krupičková, L. Láska, K. Mašek, T. Mocek, M. Pfeifer, A. Präg, O. Renner, K. Rohlena, B. Rus, J. Skála, P. Straka, and J. Ullschmied, Phys. Plasmas **8**, 2495 (2001).
[34] H. Baumhacker, G. Brederlow, E. E. Fill, R. Wolk, S. Witkowski, and K. J. Witte, Appl. Phys. B: Lasers Opt. **61**, 325 (1995).
[35] B. Rus, T. Mocek, A. R. Präg, J. C. Lagron, M. Hudeček, G. Jamelot, and K. Rohlena, J. Phys. IV **11**, 2 (2001).
[36] W. Chen, S. Wang, C. Mao, B. Chen, and A. Xu, in *1990 Conference on Lasers and Electro-Optics Technical Digest* (Optical Society of America, Washington, 1990), Vol. 7, p. 282.
[37] J. Sobota (private communication).
[38] A. Carillon, P. Dhez, B. Gauthé, P. Jaeglé, G. Jamelot, A. Klisnick, and J. C. Lagron, Proc. SPIE **1140**, 271 (1989).
[39] J. Svatos, D. Joyeux, D. Phalippou, and F. Polack, Opt. Lett. **18**, 1367 (1993).
[40] G. Jamelot, A. Carillon, P. Jaeglé, A. Klisnick, D. Ros, P. Zeitoun, P. Fourcade, S. Hubert, J. C. Lagron, L. Vanbostal, S. Sebban, F. Albert, P. Agostini, D. Garzella, P. Breger, A. Belsky, I. Kamenskikh, D. Joyeux, D. Phalippou, M. Boussoukaya, A. Zeitoun-Fakiris, G. Lacheze-Murel, and E. Béchir, IEEE J. Sel. Top. Quantum Electron. **5**, 1486 (1999).
[41] A. G. MacPhee, C. L. S. Lewis, P. J. Warwick, I. Weaver, P. Jaeglé, A. Carillon, G. Jamelot, A. Klisnick, B. Rus, P. Zeitoun, M. Nantel, P. Goedtkindt, S. Sebban, G. J. Tallents, A. Demir, M. Holden, and J. Krishnan, Opt. Commun. **133**, 525 (1997).
[42] B. Rus and T. Mocek (unpublished).
[43] R. A. London, M. Strauss, and M. D. Rosen, Phys. Rev. Lett. **65**, 563 (1990).
[44] M. C. Marconi, J. L. A. Chilla, C. H. Moreno, B. R. Benware, and J. J. Rocca, Phys. Rev. Lett. **79**, 2799 (1997).
[45] D. Joyeux *et al.* (unpublished).